https://doi.org/10.5194/hess-2023-217
Preprint. Discussion started: 16 November 2023

Hydrology and Earth System Sciences
Discussions
Open Access
EGU

HYDROLOGICAL AND PEDOLOGICAL EFFECTS OF COMBINING ITALIAN ALDER AND BLACKBERRIES IN AN AGROFORESTRY WINDBREAK SYSTEM IN SOUTH AFRICA

Svenja Hoffmeister[1], Rafael Bohn Reckziegel[2], Ben du Toit[3], Sibylle K. Hassler[1,4], Florian Kestel[5], Rebekka Maier[2], Jonathan P. Sheppard[2], Erwin Zehe[1]

[1]Institute for Water and River Basin Management, Karlsruhe Institute of Technology, Karlsruhe, 76131, Germany
[2]Institute of Forest Sciences, University of Freiburg, Freiburg, 79106, Germany
[3]Department of Forest and Wood Science, Stellenbosch University, Stellenbosch, 7602, South Africa
[4]Institute for Meteorology and Climate Research, Atmospheric Trace Gases and Remote Sensing, Karlsruhe Institute of Technology, Eggenstein-Leopoldshafen, 76344, Germany
[5]Working Group: Soil Erosion and Feedback in Research Area 1 "Landscape Functioning", Leibniz Centre for Agricultural Landscape Research, Müncheberg, 15374, Germany

Correspondence to: Svenja Hoffmeister (svenjahoffmeister@gmail.com)

Abstract. The Western Cape in South Africa is a water scarce region which under forecasted climate change scenarios may receive less rainfall and higher air temperatures. The integration of trees within agricultural systems provides an effective measure for improving water retention on agricultural land. Studying an established irrigated agroforestry system (AFS) combining alder (*Alnus cordata* (Loisel.) Duby) as a linear windbreak with a blackberry (*Rubus fructicosa* L.) crop, we explore the water use dynamics of the intercrop as influenced by the windbreak element by combining methods from hydrology, soil science and forestry. We also aim to evaluate whether the proposed experimental design is sufficient to capture the water balance and the underlying controls.

Due to the irrigation the AFS is no longer a water- but rather an energy-limited system. During the measurement period 13 rainfall events were recorded delivering 5.5 – 117.6 mm of rainfall with an intensity of 0.4 to 5.7 mm hr^{-1}. Root water uptake and event analysis show infiltration to likely occur via macro-pore flow with root water uptake occurring in two depth zones corresponding to different plant communities. Soil water content varied by depth and was influenced by physical and environmental factors, but was generally higher in the intercrop zone than within the windbreak influence zone. Soil moisture did not fall below the water content at the permanent wilting point (<-1500 kPa). Values corresponding to soil water tensions above 1000 kPa were recorded on several occasions, these were mitigated by irrigation, and thus, did not result in water stress. Nutrient distribution and soil physical properties differed near the windbreak in comparison to the blackberry crop and the carbon sequestration potential is great in comparison to monoculture farming.

The interdisciplinary work explored numerous aspects of AFS and acquired different perspectives, confirming hypotheses through cross-method analyses.

https://doi.org/10.5194/hess-2023-217
Preprint. Discussion started: 16 November 2023

Hydrology and Earth System Sciences
Discussions

1 Introduction

In a changing and challenging world, flexibility and adaptation measures are required to maintain and enhance the living standard of global citizens while facilitating ecosystem protection and restoration, as well as ensuring agricultural productivity in the light of increasing frequency of water shortages, particularly in the global south (Douville et al., 2021). One mitigation measure to address the pressing challenges in the agricultural sector is the reintegration and improvement of agroforestry systems (AFS). AFS describes the combination of woody perennial species with crops and/or livestock complements and enhances resilience and productivity of existing agricultural systems, provide new perspectives and has the potential to deliver multiple benefits (Sheppard et al., 2020a). AFS can be applied within existing agricultural land and take many temporal and spatial forms differing in composition and arrangement, examples of commonly practiced systems include: alley cropping (crops/plants are grown between rows of trees or shrubs), hedgerows and windbreaks, multi-strata agroforestry (multiple layered trees and crops), parklands, boundary planting and planted fallows (Kuyah et al., 2019). Benefits of incorporating woody perennials into agricultural systems encompass non-timber forest products, animal fodder and building materials, alongside increased household resilience (Kuyah et al., 2019; Sheppard et al., 2020a, b). Simultaneously, such systems promote a more sustainable and diversified land use (Mbow et al., 2014; Rosenstock et al., 2019; Wilson and Lovell, 2016; Jose, 2009) in contrast to conventional modern monocropping systems (Kuyah et al., 2019; Sheppard et al., 2020a). Multiple on-site environmental benefits include soil conservation, nitrogen fixation, nutrient input, improved water infiltration capacity, enhanced water quality, reduced evapotranspiration, reduced surface runoff and erosion, and stable soil fertility leading to sustainable agricultural land use (Mbow et al., 2014; Rosenstock et al., 2019).

Tree shelterbelts such as windbreaks have various impacts on the microclimate within their zone of influence, which in turn affect the water balance. The maximum zonal effect extends five times the height of the windbreak downwind and for a short distance upwind (Campi et al., 2009; McNaughton, 1988). The reduction of wind speed and shading influences evapotranspiration, air temperature and promotes dew formation, while the leaf area and branches intercept rainfall. Dew formation is increased by up to 80 %, resulting in an increase of precipitation by up to 20 % and soil moisture by up to 10 % (Nägeli, 1943; Van Eimern et al., 1964). Windbreaks have been found to reduce wind speed and potential evaporation by up to 70 % and 30 % respectively on the leeward side (Veste et al., 2020; Hintermaier-Erhard and Zech, 1997; Häckel, 1999). Such windbreak effects result in reduced wind erosion and consequently a lesser reduction in soil quality; the wind would otherwise transport the finest topsoil fractions (alongside any nutrients) away (Shi et al., 2018; Shao, 2008). Besides reducing erosion losses, windbreaks also improve nutrient cycling efficiency (Sileshi et al., 2020). Due to their small footprint, windbreaks contribute only moderately to direct carbon and nutrient enrichment, although the increased presence of woody biomass and litterfall present increased benefit over that provided by a treeless landscape. Indirectly, however, windbreaks can increase carbon storage and soil conservation through improved crop productivity (Albrecht and Kandji, 2003). However, their effect on the local water balance remains a critical research challenge.

Water availability for plants is affected by many factors, such as water supply from precipitation (climate) and irrigation (management), terrain characteristics, land use, specific soil properties and evapotranspiration potential (Lal, 2020). Soil texture, organic matter content, and aggregation state are important factors controlling soil hydraulic parameters, along with climatic and vegetation factors. The water content extracted from the water retention curves at field capacity (FC; the point at which the soil holds as much water as possible against gravity) and at the permanent wilting point (PWP; the minimum amount of soil water required that a plant does not wilt without recovery) provides an estimation of plant-available water in the pore space. Especially around FC, small fluctuations in matric potential amount to large variation in water content due to the steep slope of the water content curve around the FC. For this reason, water retention curves can be a useful tool to assess the water status and availability, especially in water-limited regions.

South Africa, particularly the Western Cape region, is a water-scarce region facing severe challenges in sustaining agricultural productivity in the future due to projected increases in air temperature and longer dry spells as a consequence of climate change

https://doi.org/10.5194/hess-2023-217
Preprint. Discussion started: 16 November 2023

Hydrology and Earth System Sciences
Discussions

(e.g. Fauchereau et al., 2003). The high wind speeds along the coastal region result in high potential evapotranspiration (PET). The connection between the potential (PET) and the actual evapotranspiration (AET) can be assessed with the Budyko framework, which is widely used for hydro-climatic classification in hydrology. It relates the annual evapotranspiration and long-term average water and energy balance on catchment or regional scales (Budyko, 1974), and can therefore, be used to categorise areas into different climate regimes, namely:

1) Energy limited settings with an aridity index (precipitation /potential evapotranspiration) > 1 and
2) Water limited settings with the aridity index < 1.

Windbreaks carry the potential to reduce the water input demand (precipitation, irrigation) ensuring sufficient water availability for crop plant growth. However, field and simulation studies investigating system-level feedbacks between trees, crops and microclimate are lacking, especially for drylands (Sheppard et al., 2020a). For this reason we tested whether a multidisciplinary and multi-method approach to characterise an established irrigated fruit orchard in South Africa is able to close this gap and deliver a holistic system perspective on the processes affecting water availability and fluxes. Specifically, we combined various campaign-based measurements from multiple disciplines with high-frequency long-term monitoring of water and energy balance components to capture both spatial variability and temporal dynamics. We used terrestrial laser scanning (TLS) technology as a novel method for investigating three-dimensional structures of trees and their shade patterns (Bohn Reckziegel et al., 2021; Raumonen et al., 2013). We took undisturbed soil samples to analyse soil physical properties, such as the site-specific water retention curve and soil hydraulic conductivity, which are key to determine the plant-available soil water storage. Transects of surface soil samples were analysed to assess the influence of the windbreak on nutrient distribution. The long-term monitoring included high-frequency soil moisture and soil water potential to provide information on temporal dynamics of potential water limitation for transpiration. This was combined with meteorological records of precipitation, solar radiation, air temperature, relative humidity and wind speed, thus, allowing for the characterisation of both water supply and potential evaporation demand and related energy limitation. The main objective of this study is to synthesize dominant controls on water availability from these observations and to particularly evaluate the positive and negative effects of the windbreak on the water and nutrient balance and cycling in the AFS. We also reflect on the feasibility of our multidisciplinary approach to characterise AFS in data-scarce regions.

2 Materials and methods

2.1 Site description

The field site is located in the Western Cape Province, South Africa, near to the city of Stellenbosch on a fruit orchard located on the southern flank of the Simonsberg (fig. 1). It is situated on a 30 % slope at an elevation of approximately 400 m above sea level. The region is dominated by a Mediterranean climate with hot, dry summers (Dec-Mar) and mild, moist winters (May-Sep) (Ndebele et al., 2020). Mean annual precipitation sum in Stellenbosch is 742 mm (Meadows, 2015). The regional wind system includes strong winds from the southeast that dominate the summer months.

https://doi.org/10.5194/hess-2023-217
Preprint. Discussion started: 16 November 2023

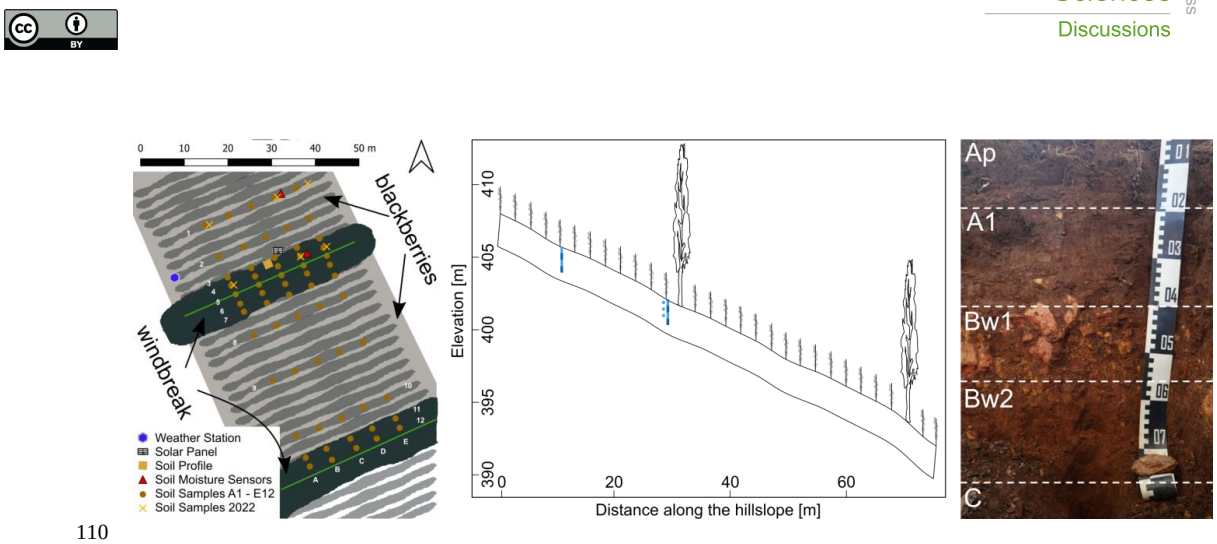

Figure 1. Left: Sampling design and location of the alder-blackberry AFS near Stellenbosch, South Africa. The triangles show the location of the soil water sensors for the monitoring, each point signifying four soil moisture sensors and three matric potential at the point near the windbreak. Middle: Transect of the slope indicating the location of soil moisture sensor stacks in the different depths (blue squares) and matric potential sensors (blue circles). Right: Photograph of the soil profile with horizon delineations and characterisation as dystric cambisol (loamic, colluvic, humic).

The study site contains multiple single tree row windbreaks of Italian alder (*Alnus cordata* (Loisel.) Duby) a non-native deciduous tree species established perpendicular to the prevailing wind direction i.e. arranged in a linear form from east-northeast to west-southwest. The studied windbreak length is 45 m and the 40 trees are planted in a regular spacing (fig. 1). The windbreak trees developed a particular oval crown shape due to the close within row spacing of the windbreak with exceptions of the last trees in the row, which developed a rounded crown on the row edge. The trees are approximately 15 to 20 years old and are pruned annually to limit encroachment on the first rows of the intercropping space. The study windbreaks spaced approximately 40 metres apart were situated within blackberry (*Rubus fructicosus* L. 'Var Waldo') fields with blackberry canes arranged in parallel rows 2 m apart and perpendicular to the slope. The 5-6 year old blackberries usually start shooting in late spring (October) and are harvested from mid-January to mid-March. One month after fruiting, they are cut back to the base. In the summer months (late November to January) a drip system provides irrigation. Approximately three days a week, each plant is irrigated with 2.3 L d^{-1}, distributed in cycles of 10 minutes. Once a year, before spring, a slow-release fertiliser is applied.

2.2 Field measurements, sampling, monitoring and laboratory analyses

A field campaign was conducted in September 2019 where the majority of the one-time sampling and measurements on site were carried out. During this campaign, the long-term monitoring equipment for water fluxes was also installed which measured between September 2019 and March 2020 (hereafter called the measurement period). An additional small scale campaign took place in March 2022 where further undisturbed soil samples were taken.

2.2.1 Meteorological measurements

Meteorological data were recorded in 10-minute intervals from mid-September 2019 until mid-March 2020 with an ATMOS 41 weather station (METER Group) in combination with a ZL6 Cloud90 data logger. Figure 1 shows the position of the weather station at the study site. The following variables were measured at two metres in height, namely: Solar radiation, precipitation, vapour pressure, air temperature, barometric pressure, horizontal wind speed and wind direction.

2.2.2 Soil sampling and laboratory analyses

During the campaign in September 2019, a representative soil profile at the research site was prepared and described with field methods following the FAO guidelines for soil description (Jahn et al., 2006). A composite sample from each identified horizon

https://doi.org/10.5194/hess-2023-217
Preprint. Discussion started: 16 November 2023

was taken for soil texture and nutrient analyses in order to classify the soil according to the World Reference Base for Soil Resources, WRB (IUSS Working, 2014) (fig. 1). Spatial topsoil (0-5 cm) sampling was carried out along five parallel downslope transects, crossing several blackberry and two alder rows (fig. 1). Per transect, 12 samples of approximately 300 g were liberated with a hand shovel, yielding a total of 60 topsoil samples. These samples were air-dried and passed through a 2 mm sieve, before transporting them to Germany for physical and chemical analyses.

From each soil sample, an aliquot was dried at 105 °C to determine residual water content. Subsequently, the samples were milled (Siebtechnik TEMA), dried again at 105 °C, and combusted at 1150 °C for total carbon and nitrogen concentrations (Vario EL cube, Elementar Analysesysteme GmbH, Langenselbold, Germany). For soil classification purposes, some laboratory analyses with air-dried soil samples were carried out. We determined pH in a 1:2 soil-solution-ratio with ultra-pure water and with a glass electrode (pH meter 704, METROHM GmbH, Filderstadt). Potential cation exchange capacity (CEC_{pot}) was determined using 1M ammonium acetate at pH 7. Exchangeable cations Ca, Mg, K, and Na were displaced with sodium acetate and measured through ICP-OE spectroscopy (Spectro Ciros CCD ICP Side- on Plasma Optical Emission Spectrometer, Kleve, Germany). Soil texture of the soil profile samples was conducted after removal of organic material with H_2O_2 (hydrogen peroxide) and chemical dispersion with $Na_4P_2O_7$ according to the sieve and pipette method (ISO 11277:2002).

Additionally, we took three undisturbed soil samples in 250 ml cylinders from a soil profile, at the surface and at depths of 0.3 and 0.5 m during the field campaign in September 2019 to determine soil hydraulic properties and some additional variables. Soil texture was determined through wet sieving of ground soil and smaller fractions were again separated with the sedimentation method after Köhn (ISO 11277:2002). Organic compounds were destroyed with the application of H_2O_2. Soil hydraulic conductivity of the undisturbed samples was measured with the Ksat apparatus (UMS GmbH, Munich). The method is based on the Darcy equation, describing a flux through a saturated porous medium as product of the driving head difference and the saturated soil hydraulic conductivity. The device records the falling head of the water supply though a highly sensitive pressure transducer, which is used to calculate the flux. Soil water retention characteristics on drying samples were measured on the same samples in the HYPROP device (UMS GmbH, München, Germany). It records total mass and matric head in two depths in the sample over time while it is exposed to free evaporation. A small fraction of the sample (about 10 g) was then transferred to the WP4C potentiometer (Decagon Devices Inc., Pullman, WA, USA), where soil water potential was measured based on a chilled mirror approach. Subsequent weighing, further drying and measuring contributed further reference points to the water retention curve.

In the second small campaign in March 2022, 12 additional undisturbed soil samples were taken and analysed in the same way as described above. We took the samples in blackberry row 1 (within the alder root zones) and 8 (as a reference without the windbreak influence) at three positions (east, mid and west). At each position we sampled at two depths, as close as possible to the surface and at 20 cm depth.

2.2.3 Monitoring of soil water dynamics

Eight TDR probes (Trime Pico IPH, IMKO GmbH, Ettlingen, Germany) were installed in two 4.2 cm diameter access tubes. Four sensors per tube were assembled stacked directly on top of each other. The sensors have a length of about 0.18 m, integrating over this depth, so four sensors per tube covered a depth of approximately 0.8 m. The lateral penetration depth of the microwave impulse of 5.5 cm yields an integration volume of approximately 3 L per sensor. The sensors were installed at two locations (fig. 1): 1) In the first blackberry row of the field, close to the windbreak, within the assumed rooting influence of the windbreak. 2) In row 8 of the blackberry field, as a control site removed from the rooting influence of the windbreak. Two additional TDR probes (Trime PICO32, IMKO GmbH, Ettlingen, Germany) with a measurement support volume of approximately 0.25 L were installed at a depth of 0.1 m next to each tube, to cover explicitly the topsoil moisture. Furthermore, we inserted three dielectric water potential sensors (MPS-2, Decagon Devices, Inc., Pullman, WA, USA) in a profile adjacent to the windbreak tube at depths of 0.1, 0.3 and 0.4 m to measure matric potential.

https://doi.org/10.5194/hess-2023-217
Preprint. Discussion started: 16 November 2023

Data were recorded at 15-minute intervals (TrueLog100, TRUEBNER GmbH, Neustadt, Germany) between 21 September 2019 and 14 March 2020 and retrieved data were checked for obvious outliers e.g. due to maintenance work and other technical disturbances. For most analyses, data were aggregated to averaged hourly data.

2.2.4 Terrestrial laser scanning and windbreak characteristics

The research site was digitised with a terrestrial LiDAR in September 2019 under negligible wind conditions. A Riegl VZ 2000i (RIEGL Laser Measurement Systems GmbH; Horn, Austria) was employed with a multiple-scan position approach to ensure a three-dimensional representation of the target vegetation and reduce the occlusion effects (Wilkes et al., 2017). As an amalgamated scanning target, the central windbreak was scanned from 32 scanning positions covering the alder trees; 14 positions were within 10 m distance from the windbreak, and up to 10 m away from each other. The remaining 18 positions were located at a distance of 15 to 25 m away, with wider scanning step between scans. Trees were scanned under leaf-off conditions, however a few trees had retained dried leaves on the inner crown from the previous vegetation season.
Values of diameter at breast-height (DBH, measured at 1.3 m) were measured manually in March 2020 and March 2022, for 17 trees within the windbreak row (eight trees left and right of the sensors with the central tree being closest to the sensors).

2.3 Data analyses

2.3.1 Meteorological data processing

The ultrasonic anemometer recorded unusually high values during heavy precipitation events. This error also occurred in some cases in the morning, likely attributed to dew formation. All events in question were referenced to the Stellenbosch airport climate station wind and gust speed were considered outliers and replaced with NA if their values seemed unreasonable. The decision process was straightforward, as most of the outliers reached the maximum measurable wind speed of 30 m s^{-1} on low wind days. The integrated cloud service was used to calculate potential evapotranspiration (PET) by using the FAO Penman-Monteith method (Allen et al., 1998) based on the observations and yielded daily values.
The aridity index (PET/P) was calculated based on Budyko (1974) for a) the whole observation period and b) the same period, but with an addition of 20 mm d^{-1} on three weekdays to account for irrigation inputs between December and March on days without precipitation.
Precipitation events were identified by an automated detection routine, which defined a precipitation amount of > 2 mm in less than six hours as a unique precipitation event and extracted start time and duration, precipitation amount and precipitation rate for each event. Precipitation events < 2 mm in six hours did not result in significant changes in topsoil moisture, and were therefore not considered.

2.3.2 Soil sample analyses

The nitrogen and carbon concentrations of the soil transect samples were considered replicates per row. Therefore, all five transect samples of one row were averaged to obtain a more robust estimate of the overall concentration distribution across the slope. The water retention curves of the profile soil samples were parameterised with the PDI model (Peters, 2014), which is a modified version of the work from Van Genuchten (1980) and Mualem (1976) and used to estimate plant-available water as the difference in volumetric water content between FC and PWP.

2.3.3 Evaluation of soil water dynamics from the monitoring data

The volumetric water content time series were used to retrieve information on root water uptake based on Guderle and Hildebrandt (2015) and changes in soil water storage during precipitation events. Daily root water uptake (RWU) was estimated from hourly water content time series with the Python package introduced by Jackisch et al. (2020). The algorithm derives RWU from stepwise diurnal changes in soil moisture between two consecutive days. RWU is assumed to be the

https://doi.org/10.5194/hess-2023-217
Preprint. Discussion started: 16 November 2023

Hydrology and Earth System Sciences
Discussions

decrease in soil moisture over the course of a day i.e. between two nights. For each water content sensor, daily soil moisture was checked and if it contained a stepwise decrease, RWU was calculated for that day as the difference in absolute soil moisture values between two nights including a nocturnal correction. If no decrease was found, RWU was not calculated and the window moved to the next day. The evaporative fraction was calculated as the ratio between actual and potential transpiration with the assumption that AET is represented by RWU.

We determined soil water storage changes by subtracting two successive soil moisture values and by multiplying by the sensor depth increment of 0.18 m. These changes were used to compare storage changes between windbreak-influenced and reference sites at the different depths and to optionally close the water balance during precipitation events.

2.3.4 Tree and windbreak characteristics

The point clouds were processed to obtain structural tree data, foliage data, and windbreak characteristics. Co-registration of scan positions was carried out using the software RiSCAN PRO 2.11.3 (*RIEGL* Laser Measurement Systems GmbH; Horn, Austria), following standard software protocol to generate project point clouds. In the single-scans, points were removed if the distance was further than 60 m from the scanning position; or the pulse deviation was greater than 10, and with calibrated reflectance lower than -10 dB and greater than 0 dB. Additionally, isolated scan points were removed as these were considered to be noise. Lastly, cubic down-sampling (25 mm voxel side) was applied to the final project point cloud.

The point cloud model of the windbreak was extracted and individual tree point clouds were manually segmented for 18 individuals in sequence, starting from one of the edges. Tree point clouds were used to model the tree structures and estimate tree parameters (e.g. diameter at breast height, 1.3 m from ground, tree height and volume) with TreeQSM v2.3.2 (Calders et al., 2015; Raumonen et al., 2013; Raumonen, 2017). After visual inspection, tree point clouds were categorized into occlusion classes with the goal of efficiently estimating the uncertainty of the tree parameters derived from the quantitative structure models (QSM). For this optimisation process, one tree in each occlusion category was randomly chosen and estimated precision was extended to all individuals in the group (Raumonen, 2017). Wood volume was converted to woody biomass by assuming a wood density of 420 kg m^{-3}, considering an average value for *Alnus sp.* (after: Worldwide 'open access' tree functional attributes and ecological database, Harja 2023). The belowground root biomass was estimated as 28.54 % of the aboveground woody biomass (Frouz et al., 2015).

The calculated leaf area index (LAI) was used to approximate cumulated interception over the course of a rain event. An empirical estimation of leaf area dependent interception storage value of 0.0001 m was applied, such a value has been used in many different modelling studies providing satisfactory estimates of the interception storage (e.g. Zehe et al. (2001)). The leaf area dependent interception storage value is multiplied with the LAI to yield interception estimations.

The shadow model by Bohn Reckziegel et al. (2021) was utilised to estimate shading effects of the windbreak through the QSMs. This enabled an estimate of the shade cast under and surrounding the windbreak under leaf-off conditions. A nominal date representing the site conditions was chosen as 25 September as experienced in the field campaign. The initially acquired QSMs were simplified with two replacement iterations (Bohn Reckziegel et al., 2022). The tree structures were bound together in a data frame to expand the model capabilities from single- to multiple-trees in a simulation. After removing four trees closest to the windbreak edge, we mirrored the retained trees for simulating a windbreak session with a total of 26 trees. The shadow model was fed with minute solar irradiance data from 2019 (January to December) provided by Stellenbosch University (Stellenbosch Weather) and derived from the Sonbesie meteorological station (33°55'42.84" S, 18°51"55.08" E, 119 m a.s.l.) less than 10 km from the research location and shadow projections were simulated on a ground surface of 0.4 ha (100 m East-West, 40 m North-South) with a grid cell size of 10 cm x 10 cm, and centralised to the windbreak position for each time interval of 10 minutes.

Measured DBH values were used to estimate the biomass gain over the course of a year, which in turn can reveal information on the alders' water use efficiency (WUE). The biomass for both days for different tree compartments (total aboveground and

https://doi.org/10.5194/hess-2023-217
Preprint. Discussion started: 16 November 2023

Hydrology and Earth System Sciences
Discussions

root) was estimated using the equation given Gholz et al. (1979) for red alder (*Alnus rubra* (Bong.)) as a proxy for *A. cordata*. The WUE is then calculated by dividing the difference in total biomass (sum of both compartments) of each year by the annual transpiration (1150 mm yr^{-1} observed by Veste et al. (2020) in 2015-2016 on a nearby vineyard). Multiplying this by the actual biomass produced based on the TLS derived parameters gives a rough idea of water usage of the alder during its lifetime (under the strong assumption that WUE is constant throughout a tree's lifetime).

3 Results

3.1 Meteorological observations

The measurement period falls within the South African summer months. The average measured air temperature was 19.5 °C with a minimum of 7.5 °C and a maximum value of 35.7 °C. A total of 245 mm of precipitation fell during the measurement period, notably 118 mm fell during one single storm event on 25 October 2019 (fig. 2, upper part). The measured wind direction within the study site was predominantly westerly in spring/early summer and easterly in late summer/autumn. Mean wind speed was 2.2 m s^{-1} and reached maximum speeds of > 30 m s^{-1} on two occasions. PET was estimated to average 5.2 mm d^{-1}, with a peak in late February of 11.2 mm d^{-1} (data not shown) and cumulative PET reached a total of 913 mm.

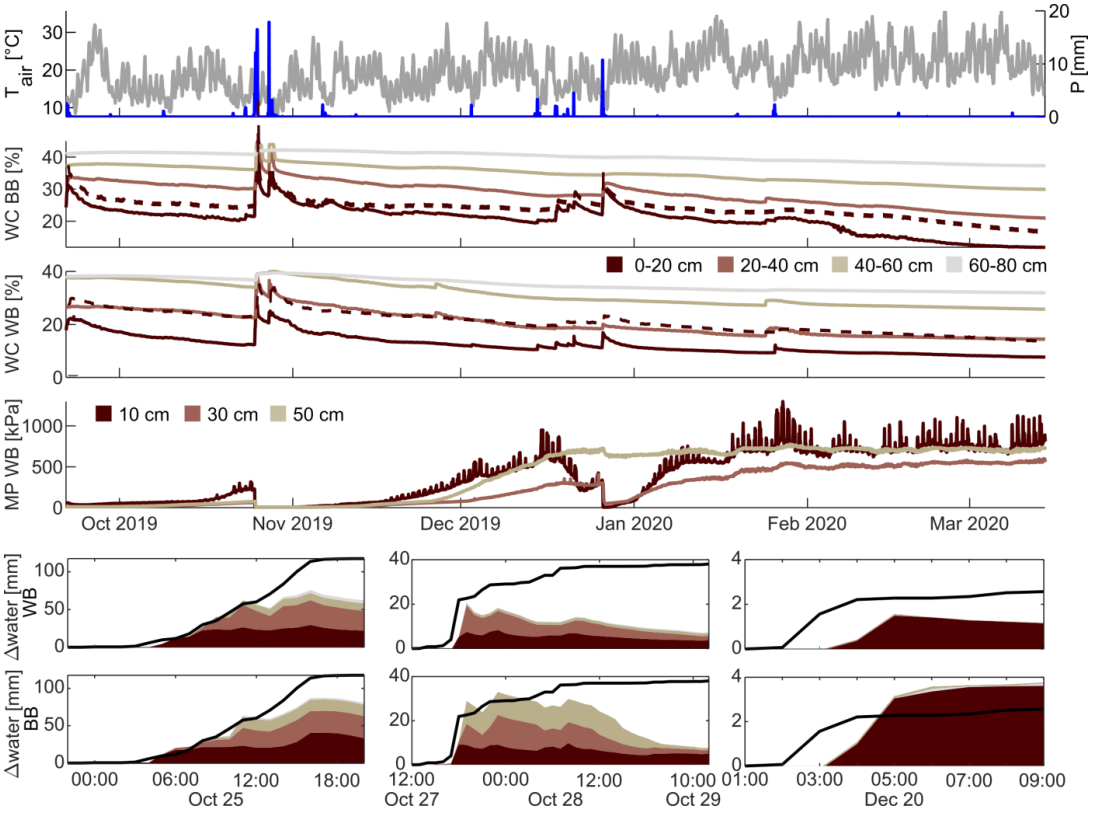

Figure 2. Meteorological observations (precipitation P, air temperature T) of the whole measurement period (upper panel). Soil moisture (volumetric water content WC) and matric potential (MP) time series at both locations (middle panels; WB: wind break, BB: blackberries). The dashed line represents the 10 cm soil moisture sensor. The lower panels show cumulative precipitation (line) and cumulative soil water storage change of each sensor for selected precipitation events, for both the windbreak (upper row) and the blackberry (lower row) location. The different colours represent the different depths of the sensors.

https://doi.org/10.5194/hess-2023-217
Preprint. Discussion started: 16 November 2023

Hydrology and Earth System Sciences
Discussions

The aridity index for the entire period was calculated to be 3.7, and with a value larger than 1, falls into the water limited/arid region of the Budyko curve. When accounting for the additional irrigation in the summer the aridity index dropped to 0.65, indicating a humid/energy limited regime.

Thirteen precipitation events > 2 mm were identified, ranging in total precipitation from 2.5 mm to 117.6 mm and in measured maximum intensity from 4.1 to 82.6 mm h^{-1} (table 1). On average most of the events had a precipitation rate of 1.6 mm h^{-1}, therefore, considered low intensity events with mean durations of 11 h 41 min. The longest event lasted 37 h.

Table 1. Observation data extracted for the precipitation (P) events above 2 mm per 6 hours (Ini = initial).

Event	Start date	Duration [hr]	P. Amount [mm]	Max. P. Rate [mm hr^{-1}]	Ini. Soil Moist. [-]
1	21 Sep 2019 11:00:00	23.0	10.5	12.2	0.51
2	08 Oct 2019 20:00:00	2.0	2.5	7.1	0.51
3	23 Oct 2019 11:00:00	6.0	4.1	22.4	0.37
4	24 Oct 2019 23:00:00	21.0	117.6	65.3	0.37
5	27 Oct 2019 13:00:00	37.0	38.1	82.6	0.59
6	06 Nov 2019 07:00:00	14.0	5.5	17.3	0.57
7	02 Dec 2019 21:00:00	3.0	2.6	9.2	0.32
8	14 Dec 2019 17:00:00	2.0	4.3	5.1	0.26
9	17 Dec 2019 17:00:00	15.0	8.5	72.4	0.26
10	20 Dec 2019 02:00:00	7.0	2.6	4.1	0.28
11	21 Dec 2019 05:00:00	1.0	4.6	10.2	0.30
12	26 Dec 2019 06:00:00	10.0	23.1	45.9	0.32
13	25 Jan 2020 21:00:00	11.0	7.1	13.3	0.24

3.2 Soil Sample analyses

3.2.1 Soil profile and undisturbed samples

The soil profile (fig. 1) was classified as Eutric Cambisol (Colluvic, Humic, Siltic) based on the international soil classification system WRB. It exhibits a silty texture across all horizons (table 2) with a high base saturation and an accumulation of colluvial material eroded from upper parts of the slope in the shallower part of the profile. The supplementary qualifier “humic” (IUSS Working, 2014) was added due to the high average carbon content within 50 cm from the mineral soil surface.

Table 2. Characteristics of the five horizons identified in the soil profile (fig. 1).

Horizon	Depth	Texture	pH (H_2O)	CEC [$mmol_c$ kg^{-1}]	Base saturation [%]	C(org) [%]	N [%]
Ap	0-20 cm	Silty Clay Loam	6.9	221	74	2.89	0.17
A1	20-40 cm	Silty Clay Loam	5.8	175	28	2.37	0.13
Bw1	40-55 cm	Clay Loam	5.0	144	20	1.22	0.08
Bw2	55-75 cm	Clay Loam	4.9	127	24	0.89	0.06
C	> 75 cm	Clay Loam	4.8	117	26	0.54	0.05

The three undisturbed profile samples taken adjacent to the soil water equipment and the additional samples collected in 2022 were analysed for soil hydraulic properties (table 3). The bulk density is overall moderate ranging from 1.01 to 1.25 g cm^{-3}

https://doi.org/10.5194/hess-2023-217
Preprint. Discussion started: 16 November 2023

Hydrology and Earth System Sciences
Discussions

except for the deepest profile sample of 1.49 g m^{-3}. In the upper samples bulk density is greater at the windbreak, hence porosity and hydraulic conductivity smaller compared to the samples in the blackberry crop.

Table 3. Laboratory analysis of three soil samples taken adjacently to the soil moisture monitoring point near the windbreak at different depths. Abbreviations are: WB P = profile, WB = windbreak, BB = blackberries, E = east, M = middle, W = west, FC = field capacity, PWP = permanent wilting point, PAW = Plant-available water. The values of the three columns from the right are estimated using the PDI water retention model (Peters, 2014). The last four rows are averages of the windbreak and berry location at the two depths.

Location	Sample Depth [m]	Hydraulic conductivity (Ksat) [mm hr-1]	Organic matter [%]	Bulk density [g cm-3]	Porosity	Wat. Cont. FC [m3 m-3]	Wat. Cont. PWP [m3 m-3]	PAW [m3 m-3]
WB P	0.0	263.1	15.1	1.17	0.56	0.426	0.178	0.248
WB P	0.3	108.7	9.3	1.11	0.58	0.367	0.136	0.231
WB P	0.5	3.2	7.3	1.49	0.44	0.393	0.169	0.224
WB E	0.05	203.3	6.6	1.19	0.55	0.368	0.165	0.203
WB E	0.28	94.05	10.2	1.16	0.56	0.396	0.168	0.228
WB M	0.05	114.5	13.9	1.19	0.55	0.364	0.174	0.191
WB M	0.26	111.4	10.3	1.18	0.55	0.335	0.164	0.172
WB W	0.05	171.9	14.2	1.19	0.55	0.373	0.175	0.199
WB W	0.23	426.6	11.5	1.12	0.58	0.358	0.179	0.179
BB E	0.10	688.8	11.9	1.01	0.62	0.322	0.158	0.164
BB E	0.25	186.8	11.5	1.25	0.53	0.379	0.180	0.199
BB M	0.10	255.7	12.7	1.06	0.6	0.327	0.169	0.158
BB M	0.25	189.3	6.9	1.21	0.54	0.393	0.176	0.216
BB W	0.10	379.8	9.7	1.13	0.57	0.346	0.178	0.168
BB W	0.25	413.1	12.0	1.04	0.61	0.331	0.170	0.161
WB	0.05	163.2	11.6	1.19	0.55	0.369	0.171	0.197
WB	0.25	210.7	10.7	1.15	0.56	0.363	0.170	0.193
BB	0.05	441.4	11.4	1.07	0.60	0.332	0.168	0.164
BB	0.25	263.1	10.1	1.16	0.56	0.368	0.175	0.192

In contrast, in the lower samples this is not observable and the parameters are rather similar with the exception of saturated hydraulic conductivity. This was seen to be slightly greater within the windbreak, here, saturated hydraulic conductivity is greatest in the shallower samples and decreases with depth, whereas within the blackberry crop it is slightly greater in the lower samples.

The organic matter content varies between 6.9 and 15.1 % (table 3) across the samples, but no clear pattern shows between the averages of the locations (11.05 ± 0.1 %). The shallower samples have larger organic matter content, which decreases with depth.

The soil water retention curves (fig. 3) of the top and bottom sample exhibit similar shapes but different porosities, whereas the middle sample is less steep and decreases more homogeneously starting at a much higher saturated water content. The deepest sample has the lowest saturated water content and porosity of 0.44, while the top sample results in a porosity of 0.56 and the middle sample of 0.58. This leads to minor differences in plant-available water (PAW, table 3), which decreases from the surface (0.26 m^3 m^{-3}) downwards (0.23 and 0.24 m^3 m^{-3}). Overall, the PAW is greater at the windbreak.

https://doi.org/10.5194/hess-2023-217
Preprint. Discussion started: 16 November 2023

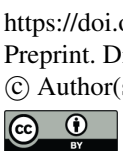

Hydrology and Earth System Sciences
Discussions

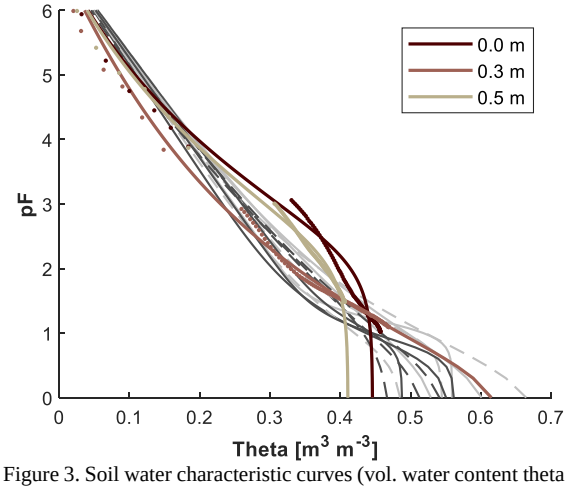

Figure 3. Soil water characteristic curves (vol. water content theta vs. soil suction pF) of undisturbed soil profile samples taken at different depths at the monitoring location within the windbreak rooting influence, adjacent to the soil moisture sensors. The values (dots) were taken during the drying process of the sample under laboratory conditions and parameterized with the PDI model (lines). Lines in grey represent additional undisturbed soil samples (darker shade are the upper samples, dashed line represents the WB samples).

3.2.2 Topsoil transect samples

Both carbon and nitrogen contents decrease with increasing distance from the alder windbreaks. The highest values reaching a carbon content of 9 % C and nitrogen content 0.6 % N are found within the windbreaks, whereas contents of 3 % C and 0.3 % N were measured farthest from the windbreaks (fig. 4). The value range of the carbon-to-nitrogen (C:N) ratio is narrower in the vicinity of the alders compared to areas situated further from the tree line.

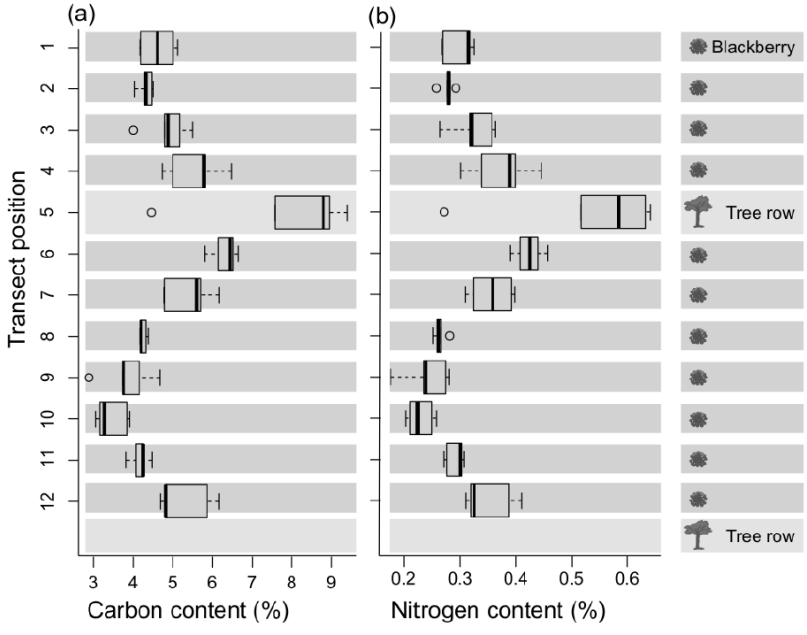

Figure 4. Carbon (a) and nitrogen (b) content of the five averaged transect topsoil (0-5 cm) samples.

https://doi.org/10.5194/hess-2023-217
Preprint. Discussion started: 16 November 2023

Hydrology and Earth System Sciences
Discussions

3.3 Soil water monitoring

3.3.1 Volumetric water content and matric potential

All sensors captured the drying processes during the summer months which generally dominate the soil moisture and matric potential measurements (fig. 2). Differences in the observations occur between location and depth. At both locations (blackberries and windbreak), the upper soil moisture sensors consistently measured less water content than the sensors at greater depths. In addition, the soil moisture values are generally slightly higher at the blackberry location (31.1 %) compared to the measurements at the windbreak (24.9 %). Reactions to rain events are observable; however, the magnitude of the reactions differs between sites, events and sensors and is described in more detailed in section 3.3.3. The matric potential observations also follow the rainfall dynamics and the drying of the soil during the summer and do not reach the PWP (pF = 4.2 or -1500 kPa). The matric potential time series of the top sensor is heavily influenced by daily fluctuations relating well to incoming solar radiation (fig. 2), which become more pronounced when the soil reaches drier conditions (< -500 kPa). The two deeper sensors also display this signal, but it is more attenuated.

3.3.2 Root water uptake

The calculation of the daily root water uptake from soil moisture observations was not successful on many days. At the windbreak location, estimation of RWU (fig. 5) was not possible for 48 % of the points (one value per sensor per day), while at the blackberry location for 56 % of all observations. At the windbreak this occurrence was most frequently observed in the topsoil (20-40 cm) whereas at the blackberry location it occurred more often for the deeper sensors (40-60 cm, 60-80 cm). These missing days are spread over the entire measurement period. Only four days had RWU estimates available from all eight sensors. A further number of days occur with no missing values per sensor location (21 days at the windbreak, 14 days at the blackberry location). On these days, we observe that at the windbreak RWU primarily occurred at the depth of 20-40 cm (44 %), whereas within the blackberry crop in the top 0-20 cm of the soil profile (70 %). RWU occurrence at the windbreak is rather uniformly distributed throughout the profile. On the four days with complete sensor data, the estimated RWU is always greater at the blackberry location when compared to at the windbreak (12 Oct.: 0.56 mm d^{-1} < 0.82 mm d^{-1}, 13 Oct.: 0.72 mm d^{-1} < 0.85 mm d^{-1}, 18 Oct. 0.66 mm d^{-1} < 1.22 mm d^{-1}, 21 Nov.: 0.4 mm d^{-1} < 1.17 mm d^{-1}).

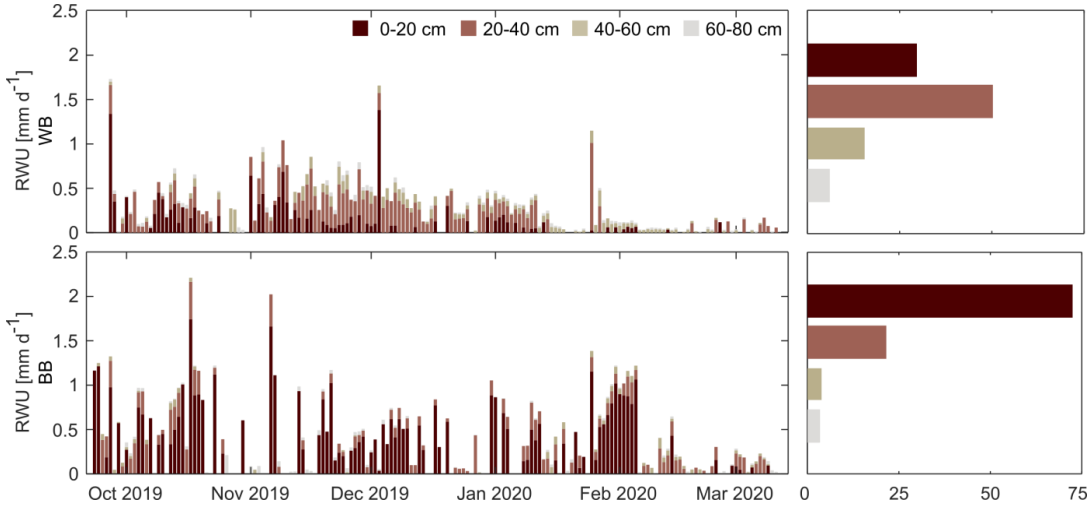

Figure 5. Stacked daily root water uptake (RWU) at the windbreak (WB) and blackberry (BB) location estimated from water content measurements at respective depth integrals. Panels on the right show how much each depth interval contributes to overall RWU [%].

https://doi.org/10.5194/hess-2023-217
Preprint. Discussion started: 16 November 2023

The evaporative fraction was calculated for the days where RWU was available for at least all four sensors at one location (29 instances) and resulted in a mean value of 0.098 (range: 0.058 – 0.223) at the windbreak and of 0.128 (0.034 – 0.230) at the berries. This indicates that transpiration is strongly water limited.

380

3.3.3 Event-based analyses

We defined a rain event as a minimum accumulated precipitation of 2 mm and uninterrupted rainfall periods of less than 6 hours. Applying these criteria, we identified thirteen distinct events during the monitoring period (fig. 2, table 1). The strongest event accumulated a total of 118 mm of rainfall within a 21 hour period and occurred on 25 October 2019. Two days later 385 another storm delivered 38 mm of rainfall over 37 hours, making it the second-largest event. Two more events with precipitation exceeding 10 mm were recorded, while the smallest event captured 2.5 mm of rainfall on 8 October 2019. Across all events, soil moisture reactions are rather immediate throughout the different sensors. Figure 2 presents a combination of accumulated precipitation and changes in cumulative soil moisture storage for some selected events (largest two events in amount of rainfall, one smaller event that shows soil moisture exceeding rainfall), highlighting variations in the reactions in 390 soil water uptake. In the two largest events (> 30 mm), a signal of increasing soil moisture is observable until the sensors at the depth of 40-60 cm. There is a difference in the timing at which the deeper sensors detect the rise in water content. On 25 October 2019 there is a gradual downward percolation of water, whereas on 28 October 2019 all three upper sensors show a simultaneous increase in soil moisture, particularly at the blackberry location. Furthermore, during the latter event, the soil did not retain the water; instead, soil moisture content rapidly declined once the precipitation ceased, which differed from the 395 behaviour in the first event.

3.4 Windbreak characterisation

3.4.1 Windbreak properties

The windbreak consists of 40 aligned trees spaced evenly and neither tree gaps nor mortality were present. Table 4 provides information on the tree structure and QSM-derived attributes. Great heterogeneity of the windbreak's tree structure shows in 400 DBH ranging from 7.7 to 33.3 cm and tree height variations between 4.3 and 13.3 m. The QSM optimisation provided precise estimates of tree heights (CV% ca. 1 %). Tree point clouds classified with high occlusion had higher uncertainties in QSM-derived tree parameters. The estimated LAI-dependent interception storage capacity yielded to 0.664 mm on the alder leaves, if assuming a LAI value of 6.64 m^2 m^{-2} based on a leaf spacing of 2.5 cm (table 4).

Excluding the edge trees, the total wood volume was found to be 617.4 L m^{-1} ("per metre of windbreak"), including 352.3 L 405 m^{-1} of branch wood. The estimated dry total biomass (trunk, branch, coarse roots) amounted to 259.3 kg m^{-1}. The variation of biomass stocks above and belowground is noted in table 4.

The calculation based on the work by Gholz et al. (1979) led to smaller values of biomass with total aboveground biomass being 95.7 kg and 99.6 kg and belowground 21.6 and 22.4 kg for the days in March of 2020 and 2021 respectively. Therefore, the incremental biomass is 4.7 kg. Dividing this by the yearly PET led to a WUE of 0.0042 g g^{-1} if considering the total biomass 410 and 0.0027 g kg^{-1} if considering only the stem biomass (such as in Dye et al. (2008)). Scaling the WUE up to the average estimated biomass of 259.3 kg per metre of windbreak estimated by the QSM optimisation results in 62,378.7 L (62.38 m^3) of water required to produce this amount of biomass.

415

https://doi.org/10.5194/hess-2023-217
Preprint. Discussion started: 16 November 2023

Hydrology and Earth System Sciences
Discussions

Table 4. Windbreak properties derived from tree data (QSM based) and additional point cloud methods.

Group	Property	Unit	Values	Description
Structure	Orientation	-	ENE-WSW	Windbreak cardinal direction in half-wind
	Tree Count	count	40	Number of trees in the windbreak
	Tree Spacing	m	1	Planting spacing (trunk-to-trunk)
	Width	m	9.46	Measured windbreak width
	Length ttt	m	39	Measured trunk-to-trunk windbreak length
	Length ctc	m	48	Measured crown-to-crown windbreak length
	Plant Coverage	-	0.819	Ratio of the min. binding box and the alpha-hull of leaf points
Volume	Trunk	L m^{-1}	128.0	Trunk volume per meter of windbreak
	Branch	L m^{-1}	352.3	Branch volume per meter of windbreak
	Root	L m^{-1}	137.1	Root volume per meter of windbreak
	Total	L m^{-1}	617.4	Total volume (trunk, branch, coarse roots) per meter of windbreak
Biomass	Aboveground	Kg m^{-1}	201.7	Aboveground biomass (trunk, branch) per meter of windbreak
	Belowground	Kg m^{-1}	57.6	Belowground biomass (coarse roots) per meter of windbreak
	Total	Kg m^{-1}	259.3	Total biomass per meter of windbreak (without leaves)
Foliage	Leaf Mass	Kg m^{-1}	3.46 ; 4.12 ; 5.12	Leaf dry mass per windbreak meter (leaf spacing 3, 2.5 and 2 cm)
	Leaf Area	m^2 m^{-1}	45.00 ; 53.69 ; 66.64	Leaf area per windbreak meter (leaf spacing 3, 2.5 and 2 cm)
	LAI	m^2 m^{-2}	5.56 ; 6.64 ; 8.24	Leaf area index (with leaf spacing 3, 2.5 and 2 cm)

3.4.2 Shade-cast simulation with the shadow model

Figure 6 illustrates the total solar radiant energy impacting the ground throughout the day on 25 September 2019. The presence of the windbreak reduces the insolation at the soil surface due to shading effects near the trees substantially (up to 75 %, close to the windbreak). These shading effects spread up to 4 m towards the north (uphill) and up to 9 m towards the south (downhill). Along the east-west axis, the shading effects are greater in size but less intense than in the north-south axis. Specific zones of minimum radiation (≈ 5 MJ m^{-2}) occur within the windbreak, mainly towards the southern side.

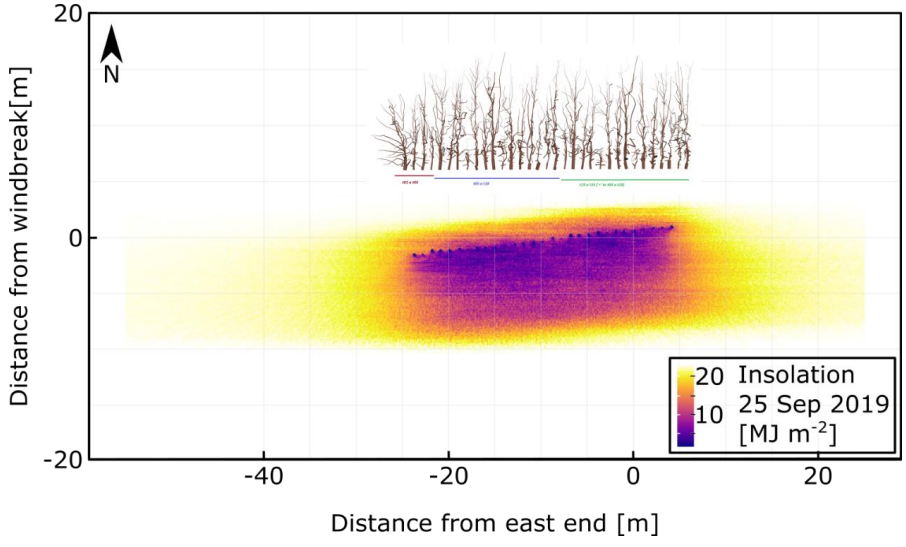

Figure 6. Insolation at ground plane modelled with the tree structures of the windbreak in leaf-off conditions for the entire day of 25 September 2019.

https://doi.org/10.5194/hess-2023-217
Preprint. Discussion started: 16 November 2023

4 Discussion

4.1 Influence of windbreak on dominant processes of the water balance

In the following we discuss the various processes of the water cycle occurring at the soil-atmosphere boundary on a plot scale and how they are influenced by the windbreak. Tracking water input, we investigate water movement into and within the soil, water redistribution and its pathway out of the study area.

4.1.1 Water input: Precipitation, irrigation, interception

The measurement period falls into the South African summer months including January, which is historically the driest month of the year with on average 16 mm (here 9.1 mm) of precipitation. The total precipitation recorded was 245 mm and partially covers the annual average of 742 mm of the region (Meadows, 2015; Veste et al., 2020). Accurate irrigation volumes and frequencies were not available, with the assumption that irrigation volumes were consistent throughout the season, the trickle irrigation system may provide a weekly water input of up to 60 mm. The irrigation amount significantly contributes to the overall water balance, exceeding the long-term average of 132 mm of the wettest month.

By intercepting rainfall, and storing part of it on leaves and branches, trees reduce the amount and velocity of water running onto the surface, and hence, its availability to vegetation below the crowns of the windbreak trees. The capacity of trees to store precipitation depends on specific characteristics, such as crown density and leaf surface area, additionally the rainfall event itself and the prevailing climatic conditions (Baptista et al., 2018; Schumacher and Christiansen, 2020). We found that the tree branch volume was approximately three times higher than the log volume, and consequently the total wood surface area was high. This indicates a strong branching of the windbreak structure, and therefore, dense vegetation (e.g. low porosity). The interception storage capacity is directly proportional to LAI, making this variable valuable for analysing different forest types and tree species, even under varying growth conditions (Schumacher and Christiansen, 2020). A LAI storage capacity of 0.664 mm per event results in a total interception of 8.5 mm for all events during the measurement period, accounting for 3.5 % of the total precipitation for the measurement period. This value is comparable to Muthuri et al. (2004) who reported 5 % interception of *Alnus acuminate* during a five-year simulation exercise. It is important to consider that our value may underestimate the total interception as events smaller than 2 mm are not considered. The LAI values were higher than those typically found in shrublands (approximately 2.0) and similar to those found in temperate and tropical forests as well as tree plantations (Bréda, 2008). Overall, we observed a higher proportion of precipitation water retained in the soil at the blackberry location in contrast to the windbreak location, where on average 63 % and 54 % of rain reached the soil column, respectively. This can be potentially attributed to interception differences between the two locations. The difference between the two locations is 26.5 mm for the entire period, which closely aligns with the interception amount of 40 mm year reported in the literature for alder species (Muthuri et al., 2004).

4.1.2 Water movement: Infiltration, surface runoff and subsurface flow

Water movement processes on, into and within the soil, such as infiltration, surface runoff and subsurface flow, can be observed during and after precipitation events, but soil physical properties can equally indicate hydrological behaviour. Infiltration determines the splitting of rainfall into surface runoff and soil water fractions. The measured topsoil Ksat (263.1 mm h^{-1}) from the soil profile samples is greater than the observed maximum precipitation intensities (max. 82.6 mm h^{-1}). High Ksat values from the undisturbed transect samples indicate favourable conditions for infiltration while Ksat exceeding precipitation intensities suggests that the soil can absorb all the precipitation. However, we did observe instances (event number 1, 5, 9, 10, 11; see also table 1) where soil water storage changes exceeded the precipitation input. The event plot in figure 2 illustrates instances where soil storage change exceeded precipitation intensity, indicating the formation of surface runoff due to saturation or infiltration excess. As a result, the absolute amount of water reaching the soil is lower, directly impacting the

https://doi.org/10.5194/hess-2023-217
Preprint. Discussion started: 16 November 2023

availability of water in the root zone (Schumacher and Christiansen, 2020), which we observed in the analysis of the precipitation events. In addition, the matric potential surpassed the FC threshold during the late October and December events, both confirming the occurrence of surface runoff. The distribution of nitrogen and carbon concentrations (fig. 4) supports this, as the enrichment around the windbreak is likely a result of a combination of erosion from downslope surface runoff and the accumulation from the trees themselves (see section 4.2.2). Similarly, downslope erosion of fine soil could also explain the unexpected observed lower Ksat values near the windbreak in the samples from 2022, which is underpinned by larger bulk density and lower porosity at the windbreak. However, we could not specifically find texture differences in the undisturbed soil samples from 2022 between the two locations that would confirm this hypothesis.

Infiltration occurs at similar rates and the flow is likely dominated by macropores, as evidenced by the immediate and minimally delayed response of the sensor at lower depths upon the onset of water input (event number 5 in table 1, bottom middle panel in fig 2). As interception reduces the amount of water entering the soil, the amplitudes of changes in soil water storage are less pronounced at the deepest windbreak sensor. In general, for most events, the cumulative water storage in the soil at both locations does not align with the recorded precipitation amount, supporting the occurrence of lateral redistribution at the soil surface or subsurface.

4.1.3 Water output: Actual evapotranspiration estimation

Root water uptake calculations did not work for approximately 50 % of the data points due to the absence of an increase in the soil moisture time series during the night, which results in a typical step-shape curve that is the necessary for RWU estimation (Jackisch et al., 2020). The influence of the irrigation on these estimations is also unclear, although it should be consistent at both locations. For these reasons, we consider the achieved RWU estimates at this site with great care.

RWU pattern differed between the two locations (fig. 5) with a higher proportion occurring in the topsoil at the blackberry location and a more evenly distributed uptake around the 20-40 cm depth within the windbreak. This indicates that the alder trees draw water from a broader range of soil horizons than the blackberry crop. The perennial blackberry plants have a main root, which can extend vertically to a maximum depth of 1.5 m (depending on soil type) and have numerous secondary roots, growing horizontally for 30-60 cm before descending vertically (Bruzzese, 1998). Alder trees are water-demanding species with high evapotranspiration rates due to the absence of mechanism to control stomatal regulation (Herbst et al., 1999). It is unclear whether the studied *A. cordata* exhibits deep rooting on the thin and rocky soils of the steep slope at our study site (80 cm soil depth at our exemplary soil profile). However, it is reasonable to assume that the species can reach the deeper soil layers due to its rooting potential. Kutschera and Lichtenegger (2002) reported that *Alnus glutinosa (L.) Gaertn*. from the same family as the *Alnus cordata* is a deep-rooting plant in waterlogged soils, with its roots reaching a depth of about 120-150 cm (Kreutzer, 1986). If the trees tap water sources below 80 cm, it would not have been captured with the installed measurement devices which in turn would explain why we observed much less water uptake at the windbreak when compared to the blackberries. Without additional information, it is difficult to determine whether the observed differences in RWU patterns are due to different rooting depths between the two species. In addition, the RWU cannot be used to estimate evapotranspiration of the windbreak. However, the evaporative fraction was estimated for days with complete sensor data and gives an idea of how much of the available energy is used for RWU, and therefore, transpiration and plant growth. For the days under consideration less RWU (evaporative fraction: 9.8 %) occurred at the windbreak in contrast to the blackberry location (evaporative fraction: 12.6 %), which could be caused by a water-limitation (or simply the installed sensors being in an incorrect location and not sufficiently capturing the RWU).

Interestingly, the Budyko aridity index indicates a shift from a water-limited to an energy-limited system when considering the additional irrigation input (changing from 3.7 without irrigation to 0.65 with irrigation). This is confirmed by the matric potential sensors, which show the plant does not reach the PWP (fig. 2), i.e. the point at which water becomes a limiting resource. The water supplied to the system by irrigation is the dominant component of the water budget and as a consequence,

https://doi.org/10.5194/hess-2023-217
Preprint. Discussion started: 16 November 2023


Hydrology and Earth System Sciences
Discussions

the AET is closer to the PET. Consequently, estimations of wind and sun shading effects can provide an idea of the AET at the field site. In fig. 6, a simulation demonstrates the windbreak's potential reduction of solar radiation on the ground, which can be up to 75 % in the immediate vicinity of the windbreak on a sunny day, as observed on 25 September 2019. The PET is estimated at 23.3 mm for the entire day from the meteorological data without shading, however, some areas of the blackberry crop did experience the shading effect of the windbreak. For instance, on the southern side of the windbreak, on a part of the field where the solar energy is reduced by 50 % for approximately 6 hours, the daily PET decreases from 23.3 to 14.8 mm d^{-1}. On the northern side of the windbreak, where the blackberries and soil are protected from the southerly winds occurring that day (depending on the distance up to a 30 % reduction in PET) assuming a 15 % reduction in PET due to wind speed reduction the PET reduces from 23.3 to 19.8 mm d^{-1}. If both effects were to occur on the same side, the cumulative impact could lead to a reduction to 12.6 mm d^{-1}, resulting in an AET that is 54 % of the PET.

While this example calculation is based solely on theoretical values and lacks actual data for comparison, it underscores the importance of the windbreak in a water-scarce region. A 30 % reduction in water demand can be crucial for the sustainability of natural and agricultural ecosystems. In a nearby vineyard, Veste et al. (2020) measured a 20 % reduction in wind speed and ET due to tree shelterbelts. For the sake of completeness, it should be noted that sunlight is essential for the growth of the blackberry crop, and excessive shading may adversely affect growth, and thus, the yield of the field, hence, a detailed assessment of shading effects is crucial for an integral assessment. It is likely that the reduction in insolation around the windbreak is shifted towards the south (downhill in the case of the given study site), as the simulation only allows shade projections on a flat terrain. Therefore, we would expect the insolation reduction to expand down the slope and decrease as one moves up the hill.

4.2 Windbreak-induced benefits for water and nutrient cycles in the landscape

4.2.1 Overall plant-available water

In contrast to our samples which displayed higher topsoil organic matter concentration but with similar PWP, Bogie et al. (2018) found significant differences in water retention at the PWP due to the potential of carbon addition to increase and stabilise aggregates in fine-grained soils alongside changes in surface properties brought about by higher CEC of organic matter in coarse soils. The PWP is also similar between windbreak and blackberry locations (both approximately 17 %) according to the similar organic matter concentrations in the undisturbed samples. The retention curves differ mainly in the wet range and are rather similar in the dry range. The spread in the wet range is greater for the lower samples, while the upper samples are grouped a bit closer together and have slightly steeper curve shapes. The soil profile samples show a clear decrease in plant-available water with depth, resulting primarily from the decrease in FC water content (table 3). In the additional samples from 2022 the topsoil plant-available water is larger at the windbreak (19.7 %) than in the blackberry crop (16.4 %), generally resulting in a higher potential to retain water in the soil near the windbreak. The deeper samples show very similar PAW (19.3 and 19.2 %). As shown in the previous section, overall less water is reaching the soil at the windbreak even though the potential to store it based on texture is greater.

Both the volumetric water content (at both locations) and matric potential (at the windbreak only) observations consistently show that the topsoil is drier than the soil at greater depths (fig. 2). The drier surface is due to evaporation of soil water combined with water withdrawal by plants from the topsoil, whereas the deep layers are not affected by evaporation and only to some extent by root water uptake. The former can be seen in the observations of the matric potential, which exhibited pronounced daily fluctuations at the surface that correlate well with the solar radiation.

The matric potential sensors did not reach the PWP of -1500 kPa during the measurement period. The uppermost sensor reached values below -1000 kPa for 53 of the 4200 data points, all occurred between January and March mostly around midday (range from 11:00 to 17:00, with an average at noon). This coincides with the times of the day when the field site is irrigated (informally for a few hours every two to three days during the summer). Both the time series of matric potential and

https://doi.org/10.5194/hess-2023-217
Preprint. Discussion started: 16 November 2023


Hydrology and Earth System Sciences
Discussions

supplemental irrigation indicate that sufficient water was available throughout the period and the plants did not experience any severe water stress.

The soil moisture time series recorded at any location frequently reached the PWP (estimated from retention curves: the top sensor at windbreak location for 86 % and top sensor at the blackberry location for 20 % of 4200 hourly data points respectively). The main difference between the locations is that at the blackberry location the PWP is reached only towards the end of summer (after 8 February), whereas, at the windbreak this limit is being reached several times throughout the observation period. We are more likely to trust the absolute values of the matric potential in this context, among other reasons because the volumetric water content sensors were used with the calibration provided by the manufacturer and not a field site specific one and susceptible to offset errors.

The trees need water for biomass growth. A rough estimation based on DBH and water use efficiency (assuming all potential energy leads to transpiration) indicates that the trees used on average around 62 m^3 of water for growing to their present size. That is on average (assuming a mean estimated age of all windbreak trees to be 17 years) 3669 L m^2 per year, clearly exceeding the yearly precipitation of 742 mm and also the water input if considering the irrigation (irrigation and precipitation: 1402 mm only for the period September to March; 1902 mm if adding irrigation to yearly precipitation). Several factors affect this approximation: 1) the trees will not maintain the same water consumption throughout their lifetime; 2) not all potential energy will result in transpiration, and therefore, water consumption of the trees.

4.2.2 Nutrient distribution and carbon sequestration potential

Possible reasons for the considerably higher nitrogen and carbon concentrations in the alder row are (a) the relocation or erosion of soil material following surface runoff in the upper and steeper parts of the slope to the flatter slope at the windbreak and (b) the continuous addition of N-rich alder biomass in form of litter fall, root exudation, and root biomass leading to higher microbial activity. Italian alder is a N-fixing tree and is able to capture atmospheric nitrogen in symbiotic root nodules (Claessens et al., 2010). There are a number of N-fixing species that seem to retard the decomposition of native soil C. Thus, this fact combined with their own root carbon productions causes the increase in soil C normally observed among N-fixing species. The bulk of the increase in soil organic carbon could come from dead roots from the alders. So, erosion is probably less important than root turnover when it comes to carbon input.

An additional potential not discussed in much detail in this study is the potential for carbon sequestration of the windbreaks in the landscape. From the terrestrial laser scans we estimated total dry biomass to 259 kg per metre. Under the rough assumption that water/woody biomass is a 50/50 split and carbon constitutes 50 % of dry biomass (Thomas and Martin, 2012); and according to the molecular weight of CO_2 we can suggest that 238 kg CO_2 equivalent (Guest et al., 2013) is sequestered in the biomass of the study alder trees. In comparison with forested land this may not be much, but as an additional carbon sink on farmland it presents a large additional potential for short to mid-term carbon storage.

5 Conclusions

Windbreaks exert major and varied effects on the surrounding crop ecosystem in AFS. Their successful implementation and proper functioning can yield multiple benefits and heavily relies on the complex water dynamics, especially in water-limited regions. We observed influences on the water balance through multiple methods utilising and analysing sensor data and soil samples.

The irrigation exerted a major influence on the water balance by transitioning the entire system from water-limited to energy-limited, ensuring sufficient water for plant growth. The windbreak themselves reduced the water demand needed for this transition by reducing soil evaporation substantially while additionally influencing processes such as interception and water redistribution. Nutrient distribution and soil physical properties differed near the windbreak in comparison to the blackberry

https://doi.org/10.5194/hess-2023-217
Preprint. Discussion started: 16 November 2023

crop and point towards nutrient accumulation by the windbreak and the occurrence of water erosion. The carbon sequestration potential of this AFS is large in comparison to monoculture farming.

Collaborative research endeavours can provide a comprehensive assessment of AFS's advantages and disadvantages. Combining methods from various disciplines draws a clearer picture of these complex systems. This interdisciplinary work explored numerous aspects of AFS and acquired different perspectives, confirming hypotheses through cross-method analyses (e.g. surface runoff detection in event-based sensor data combined with nutrient distribution analysis). The combination of additional monitoring data and repetition of campaign-based measurements with modelling studies would help with closing the water balance and might be able to fill remaining gaps and shed light on open questions regarding water fluxes in AFS.

https://doi.org/10.5194/hess-2023-217
Preprint. Discussion started: 16 November 2023

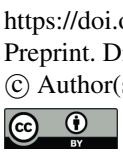

Hydrology and Earth System Sciences
Discussions
Open Access
EGU

Appendix A

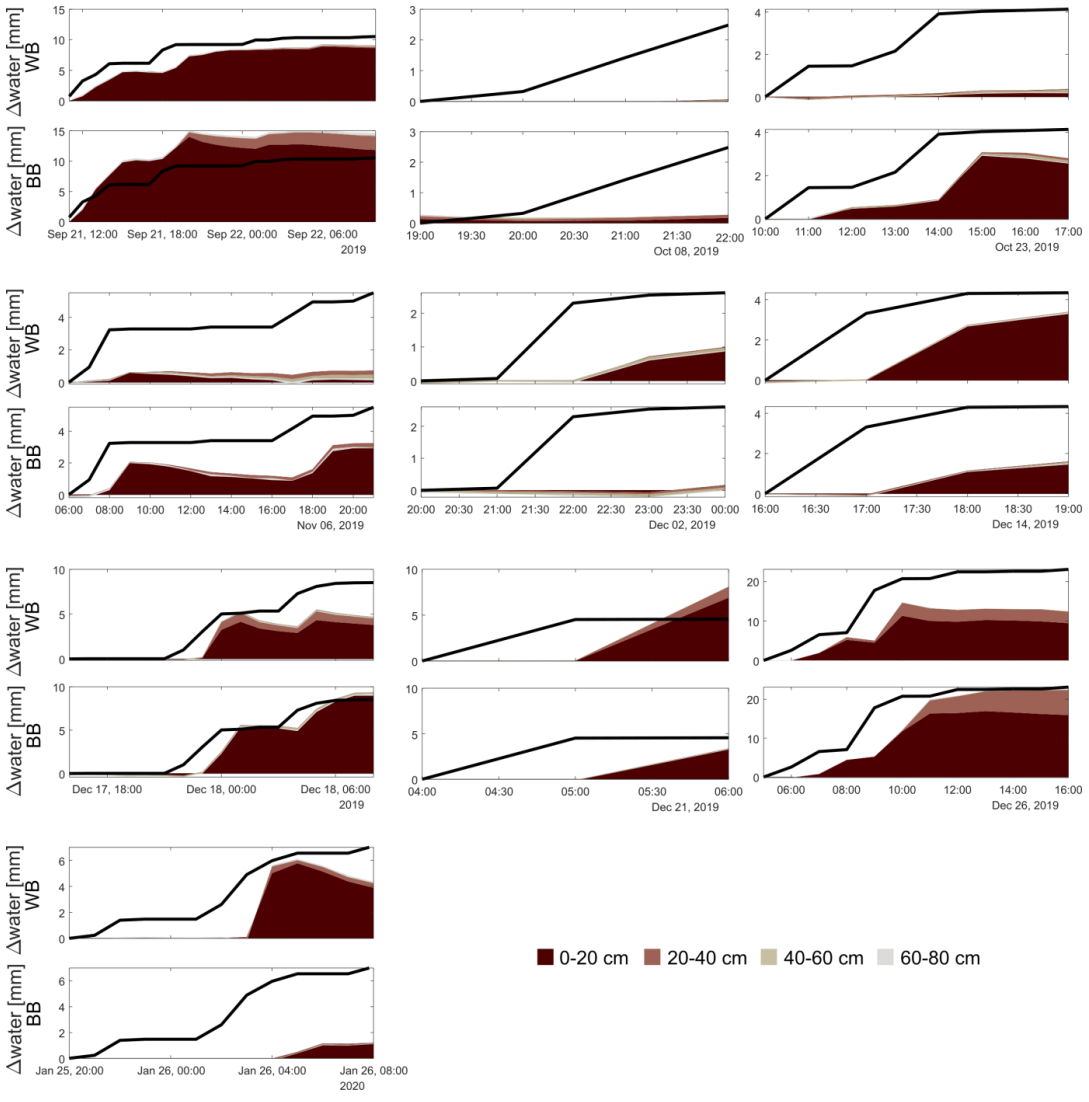

Figure A1. Panels show cumulative precipitation (line) and cumulative soil water storage change of each sensor for all precipitation events not shown in figure 2, for both the windbreak (upper row) and the blackberry (lower row) location. The different colours represent the different depths of the sensors.

Data availability

A data publication is being submitted concurrently to this submission to ESSD journal.

Author Contribution

SH, RBR, BdT, SKH, FK, RM, JPS designed their respective field methods, conducted the field work and analysed the acquired data. SH and SKH collected and curated the data of all authors. SH and EZ prepared the manuscript with contributions from all co-authors.

https://doi.org/10.5194/hess-2023-217
Preprint. Discussion started: 16 November 2023

Hydrology and Earth System Sciences
Discussions

615 **Competing interests**

One author is member of the editorial board of the journal Hydrology and Earth System Sciences.

Acknowledgements

The collection of this dataset would not have been possible without the support of Raymond O'Grady and staff at Hillcrest Berries (Pty) Ltd who permitted access and accommodated the installation of equipment and long-term measurement within a
620 working and productive farm environment. We are very appreciative of the support. We also want to acknowledge the contribution of our colleagues at the Department of Forest and Wood Science, Stellenbosch University. Namely Anton Kunneke, Deon Malherbe and Cláudio Cuaranhua who provided invaluable knowledge of the local site conditions, logistics support, and equipment maintenance as well as data download and transfer. The research was funded by the German Federal Ministry of Education and Research (BMBF) with the grant number 01LL1803.

625 **References**

Albrecht, A. and Kandji, S. T.: Carbon sequestration in tropical agroforestry systems, Agric. Ecosyst. Environ., 99, 15–27, https://doi.org/10.1016/S0167-8809(03)00138-5, 2003.

Allen, R. G., Pereira, L. S., Raes, D., and Smith, M.: Crop Evapotranspiration – Guidelines for Computing Crop Water Requirements. FAO Irrigation and drainage paper 56, Food and Agriculture Organization of the United Nations, Rome, Italy,
630 1998.

Baptista, M. D., Livesley, S. J., Parmehr, E. G., Neave, M., and Amati, M.: Variation in leaf area density drives the rainfall storage capacity of individual urban tree species, Hydrol. Process., 32, 3729–3740, https://doi.org/10.1002/hyp.13255, 2018.

Bogie, N. A., Bayala, R., Diedhiou, I., Dick, R. P., and Ghezzehei, T. A.: Alteration of soil physical properties and processes after ten years of intercropping with native shrubs in the Sahel, Soil Tillage Res., 182, 153–163,
635 https://doi.org/10.1016/j.still.2018.05.010, 2018.

Bohn Reckziegel, R., Larysch, E., Sheppard, J. P., Kahle, H.-P., and Morhart, C.: Modelling and Comparing Shading Effects of 3D Tree Structures with Virtual Leaves, Remote Sens., 13, 532, https://doi.org/10.3390/rs13030532, 2021.

Bohn Reckziegel, R., Sheppard, J. P., Kahle, H.-P., Larysch, E., Spiecker, H., Seifert, T., and Morhart, C.: Virtual pruning of 3D trees as a tool for managing shading effects in agroforestry systems, Agrofor. Syst., 96, 89–104,
640 https://doi.org/10.1007/s10457-021-00697-5, 2022.

Bréda, N. J. J.: Leaf Area Index, edited by: Jorgensen, S. E. and Fath, B. D., Gen. Ecol. Encycl. Ecol., 3, 2148–2154, 2008.

Bruzzese, E.: The biology of blackberry in south-eastern Australia, Plant Prot. Q., 13, 160–162, 1998.

Budyko, M. .: Climate and life, Academic Press, Orlando, FL, 508 pp., 1974.

Calders, K., Newnham, G., Burt, A., Murphy, S., Raumonen, P., Herold, M., Culvenor, D., Avitabile, V., Disney, M., Armston,
645 J., and Kaasalainen, M.: Nondestructive estimates of above-ground biomass using terrestrial laser scanning, Methods Ecol. Evol., 6, 198–208, https://doi.org/10.1111/2041-210X.12301, 2015.

Campi, P., Palumbo, A. D., and Mastrorilli, M.: Effects of tree windbreak on microclimate and wheat productivity in a Mediterranean environment, Eur. J. Agron., 30, 220–227, https://doi.org/10.1016/j.eja.2008.10.004, 2009.

Claessens, H., Oosterbaan, A., Savill, P., and Rondeux, J.: A review of the characteristics of black alder (Alnus glutinosa (L.)
650 Gaertn.) and their implications for silvicultural practices, Forestry, 83, 163–175, https://doi.org/10.1093/forestry/cpp038, 2010.

Douville, H., Raghavan, K., Renwick, J., Allan, R. P., Arias, P. A., Barlow, M., Cerezo-Mota, R., Cherchi, A., Gan, T. Y., Gergis, J., Jiang, D., Khan, A., Pokam Mba, W., Rosenfeld, D., Tierney, J., and Zolina, O.: Water Cycle Changes, in: Climate

Change 2021 – The Physical Science Basis. Contribution of Working Group I to the Sixth Assessment Report of the Intergovernmental Panel on Climate Change, edited by: Masson-Delmotte, V., Zhai, P., Pirani, A., Connors, S. L., Péan, C., Berger, S., Caud, N., Chen, Y., Goldfarb, L., Gomis, M. I., Huang, M., Leitzell, K., Lonnoy, E., Matthews, J. B. R., Maycock, T. K., Waterfield, T., Yelekçi, O., Yu, R., and Zhou, B., Cambridge University Press, Cambridge, United Kingdom and New York, NY, USA, 1055–1210, https://doi.org/10.1017/9781009157896.010, 2021.

Dye, P. J., Gush, M. B., Everson, C. S., Jarmain, C., Clulow, A., Mengistu, M., Geldenhuys, C. J., Wise, R., Scholes, R. J., Archibald, S., and Savage, M. J.: Water-use in relation to biomass of indigenous tree species in woodland, forest and/or plantation conditions : Report to the Water Research Commission, 2008.

Van Eimern, J., Karschon, R., Razumova, L. A., and Robertson, G. W.: Windbreaks and shelterbelts: report of a working group of the Commission for Agricultural Meteorology, 191 pp., 1964.

Fauchereau, N., Trzaska, S., Rouault, M., and Richard, Y.: Rainfall variability and changes in Southern Africa during the 20th century in the global warming context, Nat. Hazards, 29, 139–154, https://doi.org/10.1023/A:1023630924100, 2003.

Frouz, J., Dvorščík, P., Vávrová, A., Doušová, O., Kadochová, Š., and Matějíček, L.: Development of canopy cover and woody vegetation biomass on reclaimed and unreclaimed post-mining sites, Ecol. Eng., 84, 233–239, https://doi.org/10.1016/j.ecoleng.2015.09.027, 2015.

van Genuchten, M. T.: A Closed-form Equation for Predicting the Hydraulic Conductivity of Unsaturated Soils, Soil Sci. Soc. Am. J., 44, 892–898, https://doi.org/10.2136/sssaj1980.03615995004400050002x, 1980.

Gholz, H. L., Grier, C. C., Campbell, A. G., and Brown, A. T.: Equations for estimating biomass and leaf area of plants in the Pacific Northwest - research paper 41, Corvallis, Oregon, 1–38 pp., 1979.

Guderle, M. and Hildebrandt, A.: Using measured soil water contents to estimate evapotranspiration and root water uptake profiles – a comparative study, Hydrol. Earth Syst. Sci., 19, 409–425, https://doi.org/10.5194/hess-19-409-2015, 2015.

Guest, G., Bright, R. M., Cherubini, F., and Strømman, A. H.: Consistent quantification of climate impacts due to biogenic carbon storage across a range of bio-product systems, Environ. Impact Assess. Rev., 43, 21–30, https://doi.org/10.1016/j.eiar.2013.05.002, 2013.

Häckel, H.: Farbatlas Wetterphänomene, Ulmer, 1999.

Herbst, M., Eschenbach, C., and Kappen, L.: Water use in neighbouring stands of beech (Fagus sylvatica L.) and black alder (Alnus glutinosa (L.) Gaertn.), Ann. For. Sci., 56, 107–120, https://doi.org/10.1051/forest:19990203, 1999.

Hintermaier-Erhard, G. and Zech, W.: Wörterbuch der Bodenkunde, Enke, Stuttgart, 1997.

ISO 11277:2002: Soil quality — Determination of particle size distribution in mineral soil material — Method by sieving and sedimentation — Technical Corrigendum 1, 2, 2002.

IUSS Working: World Reference Base for Soil Resources. World Soil Resources Reports 106, 1–191 pp., 2014.

Jackisch, C., Knoblauch, S., Blume, T., Zehe, E., and Hassler, S. K.: Estimates of tree root water uptake from soil moisture profile dynamics, Biogeosciences, 17, 5787–5808, https://doi.org/10.5194/bg-17-5787-2020, 2020.

Jahn, R., Blume, H. P., Asio, V., Spaargaren, O., and Schád, P.: Guidelines for soil description, Rome, Italy, 2006.

Jose, S.: Agroforestry for ecosystem services and environmental benefits: an overview, Agrofor. Syst., 76, 1–10, https://doi.org/10.1007/s10457-009-9229-7, 2009.

Kreutzer, K.: The Root system of the red alder, in: Methods of productivity studies in root systems and rhizosphere organisms, edited by: Ghilarov, M. S., Kovda, V. A., Novichkova-Ivanova, L. N., Rodin, L. E., and Sveshnikova, V. M., Nauka, Leningrad, 114–119, 1986.

Kutschera, L. and Lichtenegger, E.: Wurzelatlas mitteleuropäischer Waldbäume und Sträucher, Leopold Stocker Verlag, Graz, 2002.

Kuyah, S., Whitney, C. W., Jonsson, M., Sileshi, G. W., Öborn, I., Muthuri, C. W., and Luedeling, E.: Agroforestry delivers a win-win solution for ecosystem services in sub-Saharan Africa. A meta-analysis, Agron. Sustain. Dev., 39,

https://doi.org/10.1007/s13593-019-0589-8, 2019.

Lal, R.: Soil organic matter and water retention, Agron. J., 112, 3265–3277, https://doi.org/10.1002/agj2.20282, 2020.

Mbow, C., Van Noordwijk, M., Luedeling, E., Neufeldt, H., Minang, P. A., and Kowero, G.: Agroforestry solutions to address food security and climate change challenges in Africa, https://doi.org/10.1016/j.cosust.2013.10.014, 2014.

McNaughton, K. G.: Effects of windbreaks on turbulent transport and microclimate, Agric. Ecosyst. Environ., 22/23, 17–39, https://doi.org/10.1016/0167-8809(88)90006-0, 1988.

Meadows, M. E.: The Cape Winelands, in: Landscapes and Landforms of South Africa. World Geomorphological Landscapes, edited by: Grab, S. and Knight, J., Springer, Cham., 103–109, https://doi.org/10.1007/978-3-319-03560-4_12, 2015.

Mualem, Y.: A new model for predicting the hydraulic conductivity of unsaturated porous media, Water Resour. Res., 12, 513–522, https://doi.org/10.1029/WR012i003p00513, 1976.

Muthuri, C. W., Ong, C. K., Black, C. R., Mati, B. M., Ngumi, V. W., and Van-Noordwijk, M.: Modelling the effects of leafing phenology on growth and water use by selected agroforestry tree species in semi-arid Kenya, L. Use Water Resour. Res., 4, 1–11, 2004.

Nägeli, W.: Untersuchungen über die Windverhältnisse im Bereich von Windschutzstreifen, in: Mitteilungen der Schweizerischen Anstalt für das forstliche Versuchswesen, edited by: Burger, H., Beer, Zürich, 223–276, 1943.

Ndebele, N. E., Grab, S., and Turasie, A.: Characterizing rainfall in the south-western Cape, South Africa: 1841–2016, Int. J. Climatol., 40, 1992–2014, https://doi.org/10.1002/joc.6314, 2020.

Peters, A.: Reply to comment by S. Iden and W. Durner on "Simple consistent models for water retention and hydraulic conductivity in the complete moisture range," Water Resour. Res., 50, 7535–7539, https://doi.org/10.1002/2014WR016107, 2014.

Raumonen, P.: Quantitative structure models of single trees from laser scanner data: Instructions for MATLAB-software TreeQSM, 2017.

Raumonen, P., Kaasalainen, M., Markku, Å., Kaasalainen, S., Kaartinen, H., Vastaranta, M., Holopainen, M., Disney, M., and Lewis, P.: Fast automatic precision tree models from terrestrial laser scanner data, Remote Sens., 5, 491–520, https://doi.org/10.3390/rs5020491, 2013.

Rosenstock, T. S., Dawson, I. K., Aynekulu, E., Chomba, S., Degrande, A., Fornace, K., Jamnadass, R., Kimaro, A., Kindt, R., Lamanna, C., Malesu, M., Mausch, K., McMullin, S., Murage, P., Namoi, N., Njenga, M., Nyoka, I., Paez Valencia, A. M., Sola, P., Shepherd, K., and Steward, P.: A Planetary Health Perspective on Agroforestry in Sub-Saharan Africa, One Earth, 1, 330–344, https://doi.org/10.1016/j.oneear.2019.10.017, 2019.

Schumacher, J. and Christiansen, J. R.: LiDAR Applications to Forest-Water Interactions., in: Forest-water interactions, vol. 240, edited by: Levia, D. F., Canadell, J. G., Díaz, S., Heldmaier, G., Jackson, R. B., Schulze, E.-D., Sommer, U., and Wardle, D. A., Springer, Cham, Switzerland, 87–112, 2020.

Shao, Y. (Ed.): Physics and Modelling of Wind Erosion, Springer Netherlands, Dordrecht, https://doi.org/10.1007/978-1-4020-8895-7, 2008.

Sheppard, J. P., Bohn Reckziegel, R., Borrass, L., Chirwa, P. W., Cuaranhua, C. J., Hassler, S. K., Hoffmeister, S., Kestel, F., Maier, R., Mälicke, M., Morhart, C., Ndlovu, N. P., Veste, M., Funk, R., Lang, F., Seifert, T., du Toit, B., and Kahle, H.-P.: Agroforestry: An Appropriate and Sustainable Response to a Changing Climate in Southern Africa?, Sustainability, 12, 6796, https://doi.org/10.3390/su12176796, 2020a.

Sheppard, J. P., Chamberlain, J., Agúndez, D., Bhattacharya, P., Chirwa, P. W., Gontcharov, A., Sagona, W. C. J., Shen, H. long, Tadesse, W., and Mutke, S.: Sustainable Forest Management Beyond the Timber-Oriented Status Quo: Transitioning to Co-production of Timber and Non-wood Forest Products—a Global Perspective, Curr. For. Reports, 6, 26–40, https://doi.org/10.1007/s40725-019-00107-1, 2020b.

Shi, L., Feng, W., Xu, J., and Kuzyakov, Y.: Agroforestry systems: Meta-analysis of soil carbon stocks, sequestration

https://doi.org/10.5194/hess-2023-217
Preprint. Discussion started: 16 November 2023

740 processes, and future potentials, L. Degrad. Dev., 29, 3886–3897, https://doi.org/10.1002/ldr.3136, 2018.

Sileshi, G. W., Akinnifesi, F. K., Mafongoya, P. L., Kuntashula, E., and Ajayi, O. C.: Potential of Gliricidia-Based Agroforestry Systems for Resource-Limited Agroecosystems, in: Agroforestry for Degraded Landscapes, Springer Singapore, Singapore, 255–282, https://doi.org/10.1007/978-981-15-4136-0_9, 2020.

Stellenbosch Weather: http://weather.sun.ac.za/.

745 Thomas, S. C. and Martin, A. R.: Carbon Content of Tree Tissues: A Synthesis, Forests, 3, 332–352, https://doi.org/10.3390/f3020332, 2012.

Veste, M., Littmann, T., Kunneke, A., du Toit, B., and Seifert, T.: Windbreaks as part of climate-smart landscapes reduce evapotranspiration in vineyards, Western Cape Province, South Africa, Plant, Soil Environ., 66, 119–127, https://doi.org/10.17221/616/2019-PSE, 2020.

750 Wilkes, P., Lau, A., Disney, M., Calders, K., Burt, A., Gonzalez de Tanago, J., Bartholomeus, H., Brede, B., and Herold, M.: Data acquisition considerations for Terrestrial Laser Scanning of forest plots, Remote Sens. Environ., 196, 140–153, https://doi.org/10.1016/j.rse.2017.04.030, 2017.

Wilson, M. H. and Lovell, S. T.: Agroforestry-The next step in sustainable and resilient agriculture, Sustain., 8, https://doi.org/10.3390/su8060574, 2016.

755 Worldwide 'open access' tree functional attributes and ecological database: http://db.worldagroforestry.org/, last access: 14 August 2023.

Zehe, E., Maurer, T., Ihringer, J., and Plate, E.: Modeling water flow and mass transport in a loess catchment, Phys. Chem. Earth, Part B Hydrol. Ocean. Atmos., 26, 487–507, https://doi.org/10.1016/S1464-1909(01)00041-7, 2001.